Reprinted from Preprint Volume: 13th Conference on Severe Local Storms, October 17-20, 1983, Tulsa, Okla. Published by the American Meteorological Society, Boston, Mass.

4.5

JAWS MICROBURSTS REVEALED BY TRIPLE-DOPPLER RADAR, AIRCRAFT, AND PAM DATA

T. Theodore Fujita
The University of Chicago
Chicago, Illinois

Roger M. Wakimoto
UCLA
Los Angeles, California

1. INTRODUCTION

The downburst phenomena identified in 1976 by Fujita and reported by Fujita and Byers (1977) have been studied by Projects NIMROD in 1978 and JAWS in 1982. These projects confirmed the existence of small and large downbursts which are clearly separated by temporal and spatial scales into MICROBURSTS and MACROBURSTS (Fig. 1).

In spite of the advances in mesoscale observation, analysis, modeling, and forecasting in recent years, misoscale disturbances have not been observed or experienced by a majority of meteorologists. Inadequate observations have often resulted in skepticism on the existence of sub-mesoscale disturbances.

Misometeorological analysis (MISOANALYSIS) can now be performed by combining the following mostly non-standard observations:

- Single or multiple-Doppler data
- Ground photography taken from the radar site
- Aerial measurements and photography
- Post-storm survey from the air and ground

Presented in this paper are examples of the misoanalysis of the JAWS data.

2. WET AND DRY MICROBURSTS

Not all microbursts are accompanied by measurable precipitation, 0.01" (0.25 mm) or larger. Wet and dry microbursts are defined according to the rainfall at the meteorological station beneath a microburst. Note that the frequencies of wet and dry microbursts vary significantly with geographic location.

Table 1

Wet and dry microbursts. For more statistics refer to Fujita and Wakimoto (1983).

	NIMROD	JAWS
PAM operation days	42.9 (100%)	86.1 (100%)
Microburst days	11 (26%)	49 (54%)
Wet microbursts	32 (64%)	31 (17%)
Dry microbursts	18 (36%)	155 (83%)
All microbursts	50 (100%)	186 (100%)

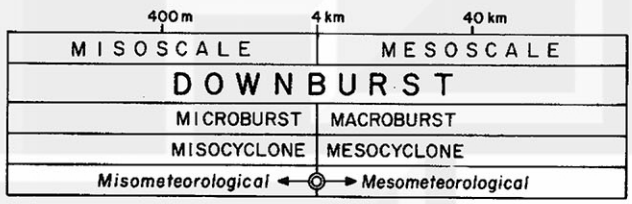

Fig. 1. Horizontal dimensions of downbursts which extend from miso- to mesoscale (Fujita, 1981).

3. MIDAIR AND SURFACE MICROBURSTS

Ground-based anemometers detect storm-induced wind shear when microburst winds reach the height of the anemometer. Based on the detectability of microbursts, they are subclassified into:

SURFACE MICROBURST: A microburst with its outburst winds detectable by a dense network of ground-based anemometers. The maximum outburst winds are located less than 100 m (300 FT) above the ground.

MIDAIR MICROBURST: A microburst aloft with its outburst winds located above the detectable height of ground-based anemometers. Within several minutes, the outburst winds may descend to the ground, turning into a surface microburst, or it may remain aloft and dissipate.

A model of the midair microburst in Fig. 2 includes inflow, downflow, and outflow winds. The maximum outflow winds blowing toward the four directions relative to the forward movement of the storm are:

V_F and V_B, front-side and back-side max winds
V_L and V_R, left-side and right-side max winds
$V_F - V_B$, front to back maximum wind shear
$V_L - V_R$, left to right maximum wind shear.

For a penetrating aircraft, the front to back or left to right wind shear along the flight path is extremely important in maintaining the airspeed.

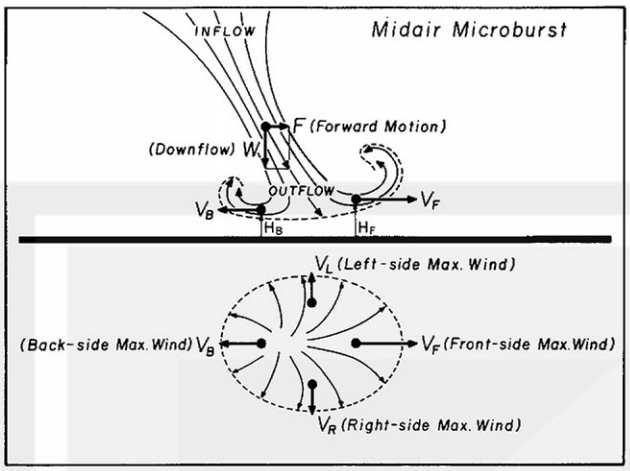

Fig. 2. A schematic view of a midair microburst in vertical (top) and horizontal planes (bottom).

As reported by the NTSB (1983), the Pan American Airlines accident at the New Orleans Airport occurred in a microburst when the aircraft encountered a 25 m/s (48 kts) back to front wind shear.

4. MIDAIR MICROBURST ON 12 JUNE 1982

A microburst descending over Denver's Stapleton Airport was monitored by the JAWS CP-3 Doppler radar (RHI sector scan) and a handheld 35 mm camera (see Figs. 3 and 4).

It should be noted that the microburst echo extended to the ground with 18 dBZ reflectivity at 10° elevation angle and 20 dBZ inside the outflow section. A few minutes earlier, the midair microburst in Fig. 5 was descending with a 25 dBZ echo at the outflow center. The left to right wind shear was 13 m/s (25 kts) which was large enough to be detected from a 15 km distance.

Both the PAM and LLWSAS winds in the Stapleton Airport beneath the midair microburst were mapped in Fig. 6. In spite of the left to right wind shear of 14 m/s (27 kts), none of the anemometers were affected by the midair microburst above the runway.

The maximum reflectivity along the CP-3 beam was plotted on the cloud photo at 1411:15 MDT to compare radar reflectivity with virga streaks. Fig. 7 shows the reflectivity of dark virga to be 25 to 33 dBZ. A 10 to 20 dBZ reflectivity, extended from the end of the virga to the ground in a slanted direction, is likely to be composed of relatively large raindrops which are transparent to visible wavelengths.

Fig. 8 shows the left to right wind shear plotted on the virga picture. Positive values, up to 18 m/s (35 kts), indicate diverging flow topped by negative values designating the converging flow at the source heights. Meanwhile, the descending velocities in the plane of the photograph, which is perpendicular to the Doppler velocities, were computed from a sequence of the 15-sec pictures. The strongest downflow at 2 to 3 km AGL was about 6 m/s (see Fig. 9).

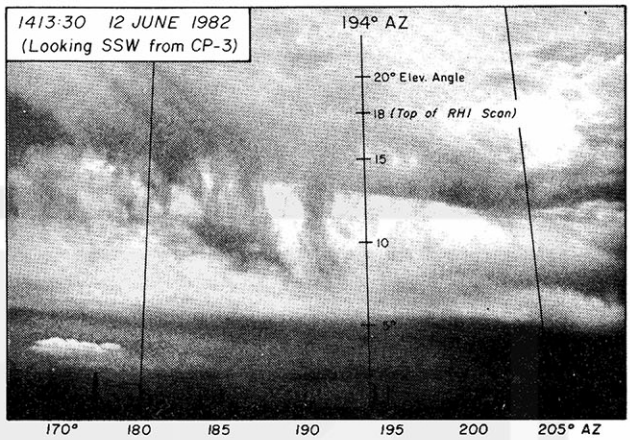

Fig. 3. Streaks of virga seen from the CP-3 site.

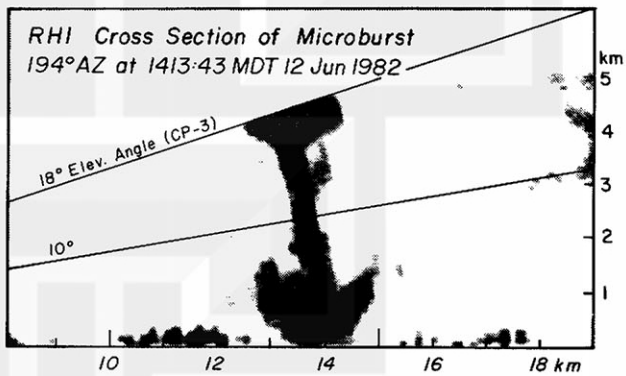

Fig. 4. An RHI cross section of the virga in Fig. 3 along the 194° azimuth.

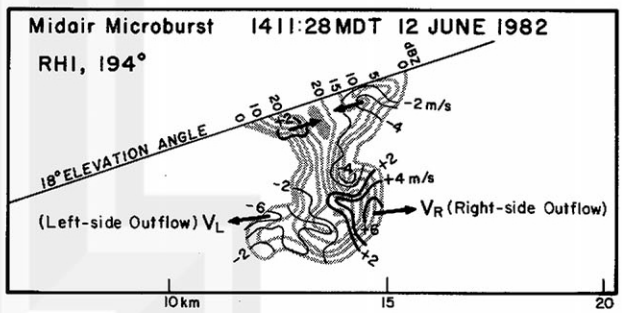

Fig. 5. An RHI cross section of a midair microburst. Both velocity and reflectivity are shown.

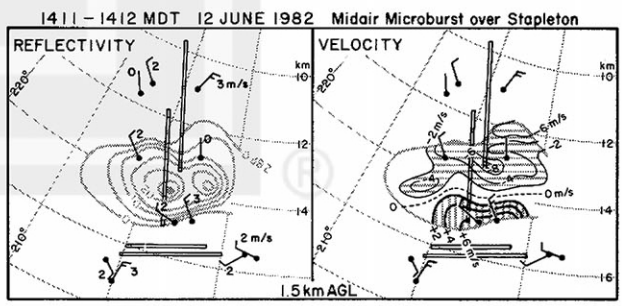

Fig. 6. Constant altitude cross section of the microburst at 1.5 km AGL. Anemometer winds are not affected by the microburst aloft.

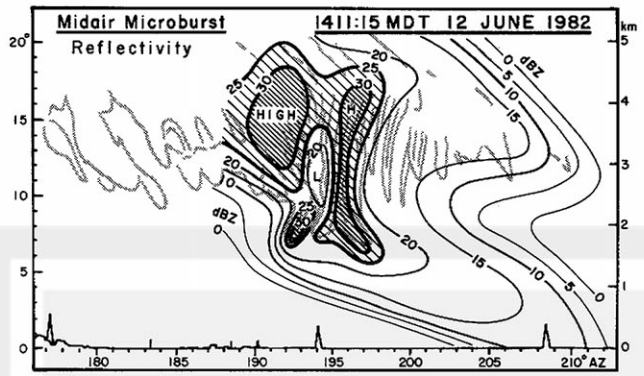

Fig. 7. CP-3 reflectivity superimposed upon the virga photo. Virga streaks were moving from right to left in the picture.

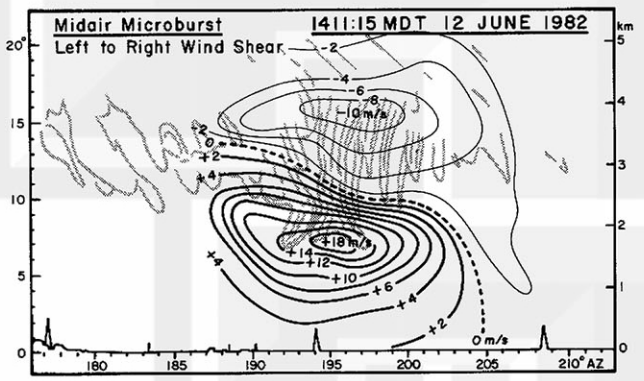

Fig. 8. Left to right wind shear inside the virga streaks. + denotes the outflow and -, the inflow.

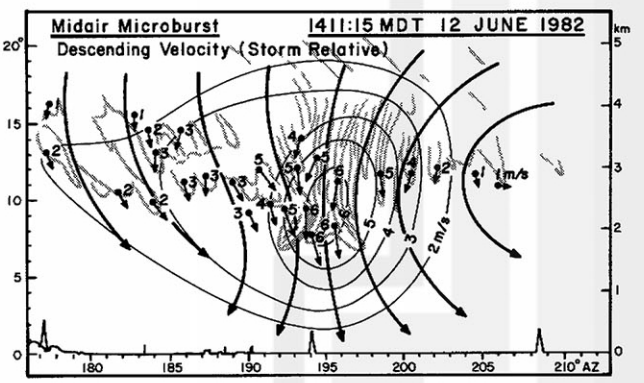

Fig. 9. Descending velocity of the virga elements computed from the picture sequence.

5. SURFACE MICROBURST ON 14 JULY 1982

A ring of dust in Fig. 10 photographed from the Wyoming King Air formed within one to two minutes. It then disappeared as rapidly as it had formed. The distribution of the dust was mapped with the aid of aerial photos taken on the following day, obtaining the 3 km diameter of the outflow (Fig. 11).

Immediately after photographing the ring of dust, the King Air flew over the dust area at 550 m (1800 ft) above the ground. Winds were

Fig. 10. Ring of dust photographed by Fujita at 1504:55 MDT on 14 July 1982, looking west.

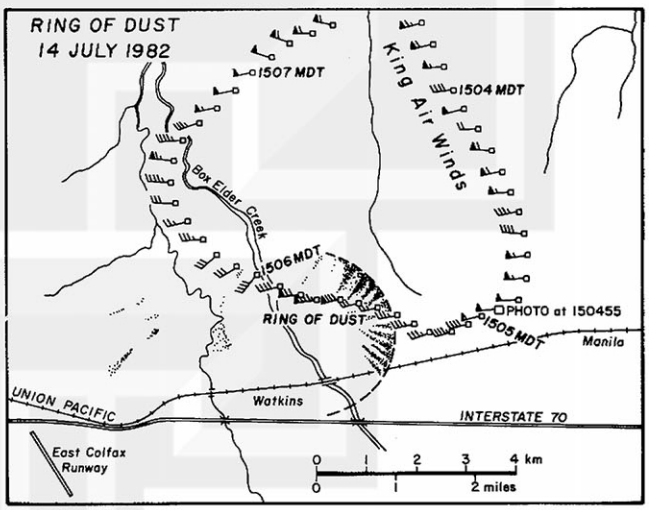

Fig. 11. Ring of dust mapped by aerial photogrammetry and the flight track of the King Air.

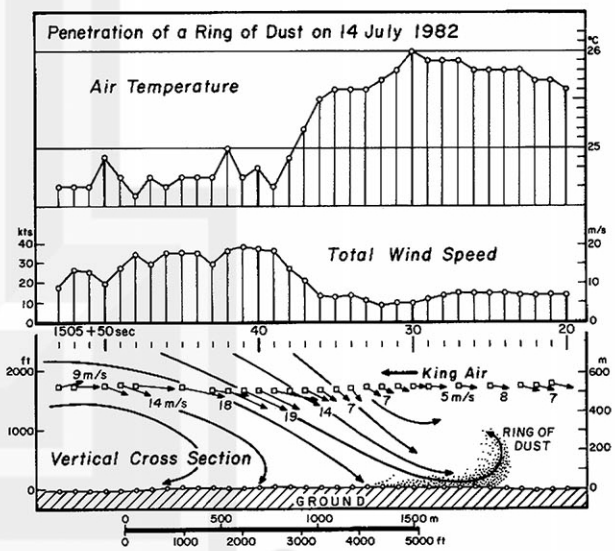

Fig. 12. King Air flight above the ring of dust in Figs. 10 and 11.

weak while flying over the blowing dust which was rising violently beneath the aircraft. Approximately one kilometer inside the dust boundary, headwind and turbulence increased suddenly and the air temperature dropped 1°C (see Fig. 12).

Several minutes before the ring of dust, from a distance of ∿40 km, JAWS CP-2 Doppler radar obtained a divergence couplet, - on the radar side and + on the opposite side. As the beam height increased, the orientation of the couplet rotated gradually, finally into a rotation couplet , - on the left side and + on the right side. The rotation couplet denotes the existence of a misocyclone. As the beam height increased, the direction of the couplet continued to rotate until it turned into a convergence couplet, + on the radar side and - on the oppposite side (see Fig. 13).

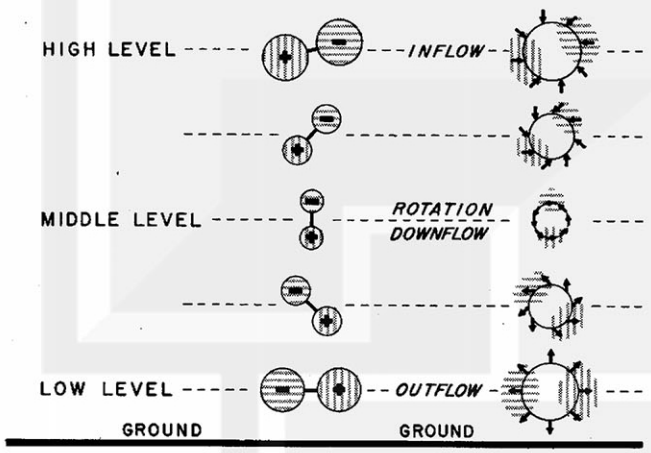

Fig. 13. Orientation of the velocity couplet with height.

Based on the orientation and the intensity of the couplet which varies with the height above the ground, the vertical distribution of the three velocities in Fig. 14 was computed. A model of a surface microburst in Fig. 15 depicts the inflow air with hydrometeors spiraling into the evaporting downflow. The rotation field of the misocyclone acts as a hydrometeor collector at high level while keeping the downflow close to its center until it hits the ground inducing a microburst outflow.

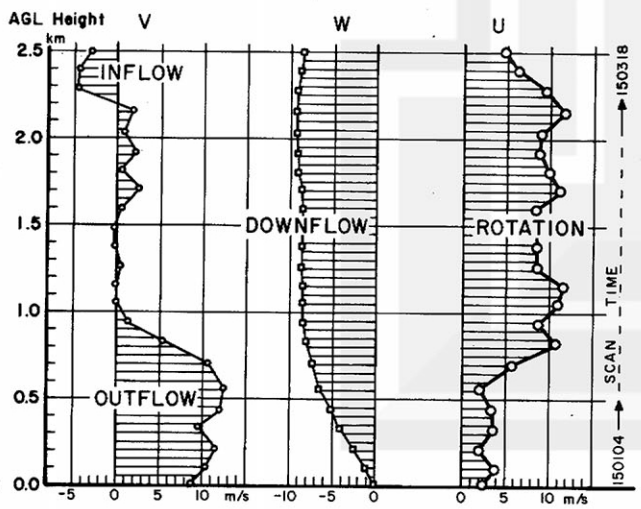

Fig. 14. Outflow, downflow, and rotation speeds computed from the velocity couplet in Fig. 13.

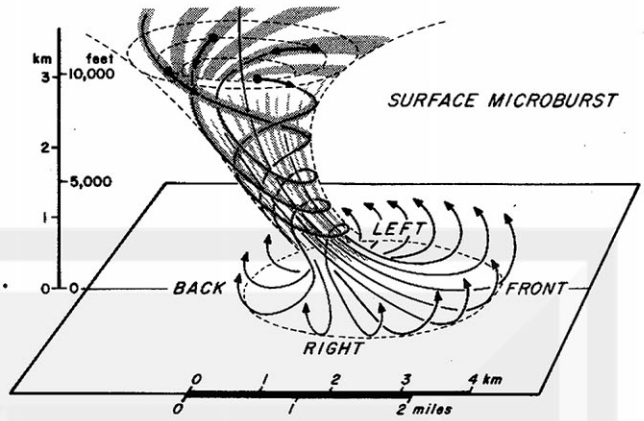

Fig. 15. A model of a surface microburst.

6. CONCLUSIONS

Misometeorological analysis of the JAWS data revealed that the source region of microbursts is characterized by weak circulations. Due to the concentration of vorticity, the downflow at middle levels is encircled by misocyclones which are mostly cyclonic but some are anticyclonic. The outflow field near the base of the midair microburst can be detected by a single Doppler radar from 10 to 40 km irrespective of the viewing direction, making it possible to detect microbursts several minutes before they descend to the ground.

Acknowledgements

This research has been sponsored by NSF under grant NSF/ATM 8109828, by NOAA under grant NA80AA-D-00001 and by NASA under grant NGR 14-001-008.

REFERENCES

Fujita, T.T., 1981: Tornadoes and downbursts in the context of generalized planetary scales. J. Atmos. Sci., 38, 1511-1534.

Fujita, T.T., and H.R. Byers, 1977: Spearhead echo and downburst in the crash of an airliner. Mon. Wea. Rev., 105, 129-146.

Fujita, T.T., and R.M. Wakimoto, 1983: Microbursts in JAWS depicted by Doppler radars, PAM, and aerial photographs. Preprints, 21st Conf. on Radar Meteorology, Edmonton, Amer. Meteor. Soc.

National Transportation Safety Board, 1983: Aircraft accident report: Pan American World Airways, Inc., Clipper 759, Boeing 727-235, N4737, New Orleans International Airport, Kenner, Louisana, July 9, 1982. NTIS PB83-910402, 113 pp.